Physics and Imaging in Radiation Oncology 32 (2024) 100653

Contents lists available at ScienceDirect

Physics and Imaging in Radiation Oncology

journal homepage: www.sciencedirect.com/journal/physics-and-imaging-in-radiation-oncology

Original Research Article

Reduced-distortion diffusion weighted imaging for head and neck radiotherapy

Eric Aliotta [a,*], Ramesh Paudyal [a], Alex Dresner [d], Amita Shukla-Dave [a,b], Nancy Lee [c], Laura Cerviño [a], Ricardo Otazo [a,b], Victoria Y. Yu [a]

[a] Department of Medical Physics, Memorial Sloan Kettering Cancer Center, New York, NY, United States
[b] Department of Radiology, Memorial Sloan Kettering Cancer Center, New York, NY, United States
[c] Department of Radiation Oncology, Memorial Sloan Kettering Cancer Center, New York, NY, United States
[d] Philips Healthcare, the Netherlands

A B S T R A C T

Background and purpose: Quantitative Diffusion Weighted Imaging (DWI) has potential value in guiding head and neck (HN) cancer radiotherapy. However, clinical translation has been hindered by severe distortions in standard single-shot Echo-Planar-Imaging (ssEPI) and prolonged scan time and low SNR in Turbo-Spin-Echo (ssTSE) sequences. In this study, we evaluate "multi-shot" (ms) msEPI and msTSE acquisitions in the context of HN radiotherapy.

Materials and methods: ssEPI, ssTSE, msEPI with 2 and 3 shots (2sEPI, 3sEPI), and msTSE DWI were acquired in a phantom, healthy volunteers (N=10), and patients with HN cancer (N=5) on a 3-Tesla wide-bore MRI in radiotherapy simulation RF coil setup, with matched spatial resolution (2x2x5mm) and b = 0, 200, 800 s/mm^2. Geometric distortions measured with deformable vector field (DVF) and contour analysis, apparent diffusion coefficient (ADC) values, and signal-to-noise-ratio efficiency (SNR_{eff}) were quantified for all scans.

Results: All techniques significantly ($P<1x10^{-3}$) reduced distortions compared with ssEPI (DVF_{mean} = 3.1 ± 1.3 mm). Distortions were marginally lower for msTSE (DVF_{mean} = 1.5 ± 0.6 mm) than ssTSE (1.8 ± 0.9 mm), but were slightly higher with 2sEPI and 3sEPI (2.6 ± 1.0 mm, 2.2 ± 1.0 mm). SNR_{eff} reduced with decreasing distortion with ssEPI=21.9 ± 7.9, 2sEPI=15.1 ± 5.0, 3sEPI=12.1 ± 4.5, ssTSE=6.0 ± 1.6, and msTSE=5.7 ± 1.9 for b = 0 images. Phantom ADC values were consistent across all protocols (errors ≤ 0.03x10^{-3}mm^2/s), but *in vivo* ADC values were ~ 4 % lower with msEPI and ~ 12 % lower with ssTSE/msTSE compared with ssEPI.

Conclusions: msEPI and TSE acquisitions exhibited improved geometric distortion at the cost of SNR_{eff} and scan time. While msTSE exhibited the least distortion, 3sEPI may offer an appealing middle-ground with improved geometric fidelity but superior efficiency and *in vivo* ADC quantification.

1. Introduction

Diffusion Weighted Imaging (DWI) is a quantitative Magnetic Resonance Imaging (MRI) technique that can non-invasively characterize head and neck (HN) cancer by measuring the Brownian motion of water. Elevated cell densities within tumors and nodal metastases cause diffusion to become increasingly restricted and this can be captured by diffusion sensitizing gradients [1]. Quantitative parameters derived from DWI such as the apparent diffusion coefficient (ADC) are meaningful surrogates for tumor cellularity [2], making it a natural candidate for guiding personalized radiotherapy strategies. Numerous applications have been proposed, including treatment response prediction [3–5] and monitoring [6–9], nodal metastasis identification [10,11], and local dose escalation guidance [12].

Despite this promise, current DWI acquisitions have limitations that hinder use in radiotherapy planning. The main challenge is that conventional single-shot echo planar imaging (ssEPI) readouts are prone to substantial image distortions. ssEPI is efficient because it captures all of 2D k-space in one "shot", but this leads to error propagation near magnetic field inhomogeneities, resulting in distortions. Distortions can exceed 1 cm in magnitude in the HN [13], which is not acceptable for use in radiotherapy planning [14].

Alternative techniques are needed to enable widespread use of DWI in radiotherapy applications. One available option is single-shot turbo-spin-echo (ssTSE) DWI [15,16], which largely eliminates distortions with repeated refocusing pulses during readout. A challenge in TSE-based DWI is that strong diffusion encoding gradients can violate the Carr Purcell Meiboom Gill (CPMG) conditions, making echo trains unstable in the presence of motion. This can be mitigated by removing non-CPMG signal components [15] or by Split Acquisition of Spin Echo and

* Corresponding author at: Department of Medical Physics, Memorial Sloan Kettering Cancer Center, 1275 Yorke Avenue, Box 84, New York, NY 10065, United States.
E-mail address: aliottae@mskcc.org (E. Aliotta).

https://doi.org/10.1016/j.phro.2024.100653
Received 7 June 2024; Received in revised form 19 September 2024; Accepted 19 September 2024
Available online 23 September 2024

Table 1
Acquisition parameters used for each DWI protocol. TE=echo time, TR=repetition time. NSA=number of signal averages. SENSE=Sensitivity Encoding. SPAIR=Spectral Attenuated Inversion Recovery, SPIR=Spectral Presaturation with Inversion Recovery. MultiVane % controls the number of rotating PROPELLER blades wherein a value of 100 % results in a scan with acquisition time equivalent to a corresponding cartesian scan. *TE values reported for ssTSE and PROPELLER refer to the effective TE which describes the timing of the central k-space echo. Additional TSE parameters for both protocols are (ssTSE/PROPELLER): TSE echo spacing = 9.4/7.0 ms, shot duration = 322/132 ms. Note that the reported scan times reflect a consistent number of averages for all b-values, while in practice one would typically acquire more signal averages at higher b-values and fewer for low or zero b-values which can substantially reduce scan times for all DWI techniques.

	ssEPI	2sEPI	3sEPI	ssTSE	PROPELLER
Resolution [mm]	2.0 x 2.0 x 5.0				
FOV [mm]	220 x 220				
Phase encode direction	Anterior/Posterior				Radial
Slices	20	20	20	20	20
TE/TR [ms]	56/3333	52/3333	50/3333	100*/8383	80*/2080
Parallel Imaging Factor (SENSE)	3	3	3	2.5	2.5
Fat suppression	SPAIR	SPAIR	SPAIR	SPIR	SPAIR
b-values [s/mm^2]	0, 200, 800				
NSA	5	5	5	5	3
EPI Shots	1	2	3	–	–
Echo train length	43	21	15	44	12
Bandwidth [Hz]	32.8	65.7	92.9	555.2	395.8
EPI frequency encode Bandwidth [Hz/]	1976.5	2586.6	2584.3	–	–
MultiVane %	–	–	–	–	250 %
Scan Time as-acquired [min:sec]	2:20	4:33	6:47	6:17	13:23
Scan time per average [min:sec]	0:28	0:55	1:21	1:15	4:28

Stimulated Echo (SPLICE) [16], which maintains comparatively higher signal-to-noise-ratios (SNR). Unfortunately, TSE still results in substantially lower SNR and longer scan times than ssEPI, as well as image blurring from T2 decay during lengthy readouts. These challenges limit achievable spatial resolutions, maximum diffusion encoding factors (b-values), and image quality. These limitations are further exacerbated in radiotherapy applications due to limitations in coil selection to accommodate patient immobilization [17] and limited hardware capabilities on hybrid MRI-linear accelerator systems [18,19].

Another approach for reduced-distortion DWI is a "multi-shot" readout which breaks up acquisitions into multiple, shorter blocks that are individually less susceptible to distortions or blurring. Multi-shot strategies have been applied to both EPI and TSE acquisitions through msEPI [20,21] and msTSE approaches such as non-Cartesian Periodically Rotated Overlapping ParallEL Lines with Enhanced Reconstruction (PROPELLER) [22,23]. These approaches can alleviate distortions without the limitations of ssTSE, but with additional tradeoffs. msEPI maintains the SNR advantages of ssEPI and can therefore facilitate low-distortion imaging with the potential for high spatial resolutions. msEPI can also reduce blurring compared with ssEPI by shortening readouts (and reducing T2* decay). However, this approach increases motion sensitivity due to inter-shot phase discrepancies resulting from strong diffusion encoding gradients and must be carefully corrected [20,24]. Furthermore, msEPI may not sufficiently remove distortions for radiotherapy applications, particularly if only a small number of shots is used. More shots can be used to further reduce distortions, but at the cost of longer scans. Similarly, PROPELLER can reduce blurring and facilitate higher SNR than ssTSE while maintaining low levels of distortion, but with prolonged scan times.

It is evident that msEPI and PROPELLER acquisitions have potential to improve the utility of DWI for HN radiotherapy, but they have not previously been benchmarked for this application. The purpose of this study is to quantify relevant tradeoffs between techniques including distortions, SNR, scan efficiency, and ADC quantification to identify an optimal strategy for HN radiotherapy. Each of these characteristics was assessed in phantom and in-vivo studies.

2. Methods

2.1. Protocol design

All imaging was performed on a 3.0 Tesla wide-bore Philips Ingenia Elition scanner (Philips Healthcare, Amsterdam, Netherlands, software version R5.7.1.2). Five DWI protocols were developed: 1) ssEPI; 2) msEPI with 2 shots (2sEPI); 3) msEPI with 3 shots (3sEPI); 4) ssTSE using SPLICE; and 5) msTSE with SPLICE PROPELLER. Acquisition details for each protocol are shown in Table 1. msEPI acquisitions used interleaved shot segmentation along the phase-encode direction with navigator-based inter-shot phase correction. All scans were axial and had three orthogonal diffusion-encoding directions. 5 signal averages were acquired for all scans except for PROPELLER, which used 3 averages to maintain reasonable scan times while also accounting for some inherent signal averaging due to oversampling of central k-space in the PROPELLER sequence. Averaging was performed on magnitude images, which were independently exported from the scanner. Repetition time (TR) was matched between EPI protocols, but echo times (TE) were individually minimized (TE range = 50–56 ms). Fat-suppression was applied in all protocols, but for *in-vivo* EPI acquisitions, saturation bands were additionally used to suppress the residual fat signal from the anterior and/or posterior neck. Signal averages were acquired equivalently for all b-values to accommodate quantitative SNR analysis, but in practice more signal averages would only be needed at higher b-values with only minimal averaging for low/zero b-values.

A T2-weighted, fat-suppressed sequence was also utilized to provide a geometric reference scan for assessing anatomical distortions in DWI. This protocol consisted of a 2D multislice, Cartesian multi-shot TSE acquisition with 2D distortion correction, a 272x272mm in-plane field of view, 1x1x3mm voxel size, bandwidth = 179 Hz, enough slices to cover the anatomy of interest (or phantom), and TR/TE=5465 ms/71 ms.

2.2. Phantom imaging

All protocols were acquired in a quantitative imaging biomarkers alliance (QIBA) diffusion MRI phantom [25] consisting of 13 cylindrical vials with varying concentrations of polyvinylpyrrolidone and known ADC values. The phantom was prepared in an ice bath according to manufacturer specifications to ensure an internal temperature of 0 °C. The phantom was immobilized in a standard HN coil for imaging. The entire scan session was repeated three times (1–2 months between scans) to assess measurement repeatability.

2.3. Volunteer imaging

Healthy volunteers (N=10) were enrolled in an IRB-approved study after informed consent. Subjects were imaged head-first supine with a foam headrest in place to maintain a comfortable neck flexion. A two-piece Flex-L surface loop coil (1 channel per piece) was placed on either side of the neck, and a flexible 16-element anterior body coil was placed atop an adjustable coil bridge elevated above the entire anatomy. The built-in 12-channel posterior coil was also used, resulting in 30 available coil channels. This setup mimicked radiotherapy simulation which uses an immobilization mask that is incompatible with a conventional HN coil.

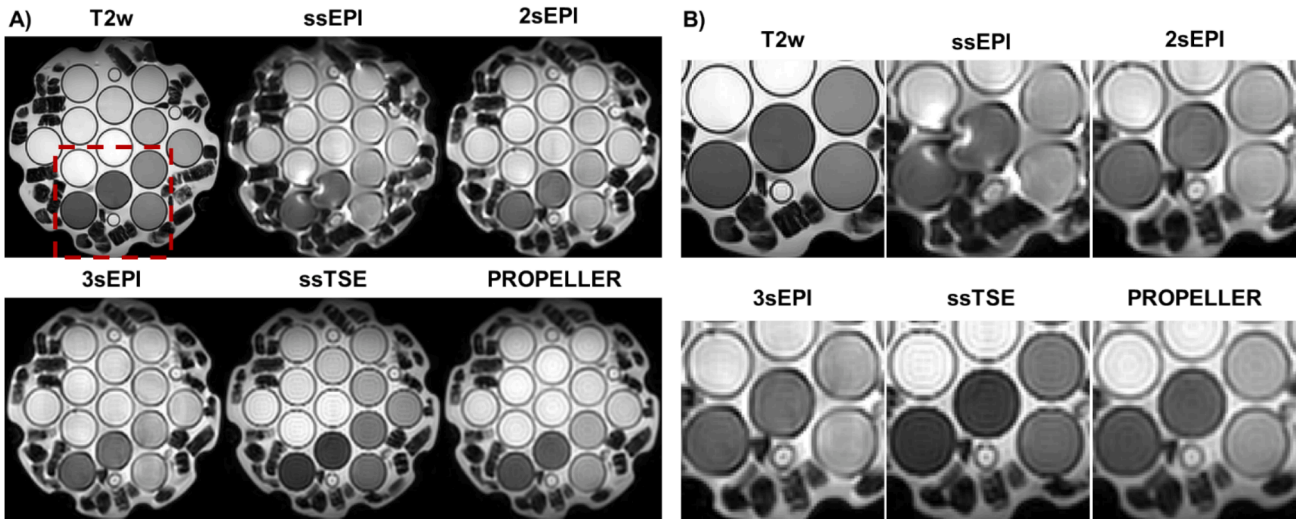

Fig. 1. Diffusion Phantom images acquired with each protocol (shown for b = 0) as well as a non-DWI T2-weighted (T2w) turbo spin echo sequence. Localized distortions were clearly visible with the ssEPI scan (likely near an inadvertent air pocket), which were reduced considerably with 2sEPI, further with 3sEPI, and effectively eliminated with ssTSE and PROPELLER.

2.4. Patient imaging

Patients with human papillomavirus-associated (HPV+) oropharyngeal cancer (OPC) (N=5) undergoing radiotherapy treatment planning were imaged after informed consent for research scans. To maintain reasonable scan times, only ssEPI, 3sEPI, and PROPELLER (Table 1) were acquired in patients.

2.5. Distortion analysis

Distortion was quantified for each DWI acquisition compared to T2 reference scan using both contour analysis and deformable image registration:

2.5.1. Contour analysis

Several structures were first delineated on T2 scans by two experienced medical physicists (EA, VY) using MIM software (MIM, Cleveland, Ohio). In phantom scans, the 13 cylindrical phantom vials were manually contoured. In humans, the parotid glands, submandibular glands, mandible, oral cavity, spinal cord, and gross tumor volume (GTV, patients only) including primary tumor (GTVp) and nodal metastases (GTVn) were contoured. GTV contours were drawn by treating radiation oncologist on a planning CT and propagated to MRI by the medical physicists.

Structures were then propagated from T2 to b = 0 reference DWI scans and adjusted manually. Agreement between structures as defined on T2 and DWI were then quantified using the Dice coefficient (i.e., the fractional overlap between structures) and the mean / 95th percentile Hausdorff distance (i.e., the mean / 95th percentile distance between structure boundaries, HD_{mean} / HD_{95}).

2.5.2. Registration analysis

Each DWI b = 0 scan was deformably registered to the T2 scan using a b-spline mutual-information algorithm (Elastix[26]). Displacement vector field (DVF) maps were extracted from deformable registrations to describe local distortions. Mean and 95th percentile displacement magnitudes (DVF_{mean}, DVF_{95}) were computed within each delineated structure.

2.6. SNR analysis

SNR maps were generated for each DWI acquisition and b-value by computing the mean (μ) and standard deviation (σ) image intensity across individual averages at each voxel (SNR=μ/σ at each voxel). Mean SNR values were computed for each technique and structure and compared between acquisitions. SNR efficiency (SNR_{eff}) was then computed by normalizing against scan time for each technique ($SNR_{eff} = SNR/T^{1/2}$ where T=scan time for one average).

2.7. ADC analysis

ADC maps were generated from each DWI acquisition using mono-exponential fitting to all acquired b-values ($S_b = S_0 e^{-bADC}$, where S_b = signal with b-value = b, S_0 = signal with b = 0).

Mean phantom ADC values were computed in the central 3 slices of each vial, and ADC values from each DWI method were compared against known values via percentage ADC differences within each vial. ADC repeatability was assessed using the repeated acquisitions by computing the interscan correlation coefficient and within-subject coefficient of variation (wCV=standard deviation across repetitions / mean across repetitions) of ADC values in each vial[27]. wCV were compared between each technique and ssEPI (across all vials).

For *in-vivo* scans, mean ADC values were computed within each delineated structure and compared between acquisitions.

2.8. Statistical analysis

Most statistical comparisons were performed using one-way analysis of variance (ANOVA) across DWI acquisitions. However, when statistically significant differences were observed with ANOVA ($P<0.05$), comparisons were performed between individual techniques using paired t-tests to identify the sources of variation. Bonferroni corrections were applied to pairwise tests to account for multiple comparisons.

3. Results

3.1. Phantom imaging

Phantom images are shown in Fig. 1. Localized distortions were clearly visible in the ssEPI acquisition but were visibly improved with 2sEPI, further improved with 3sEPI, and virtually eliminated with ssTSE and PROPELLER. This was also observed in quantitative distortion results (Supplementary Table S1), wherein all measures of distortion from 3sEPI, ssTSE, and PROPELLER were significantly lower than ssEPI

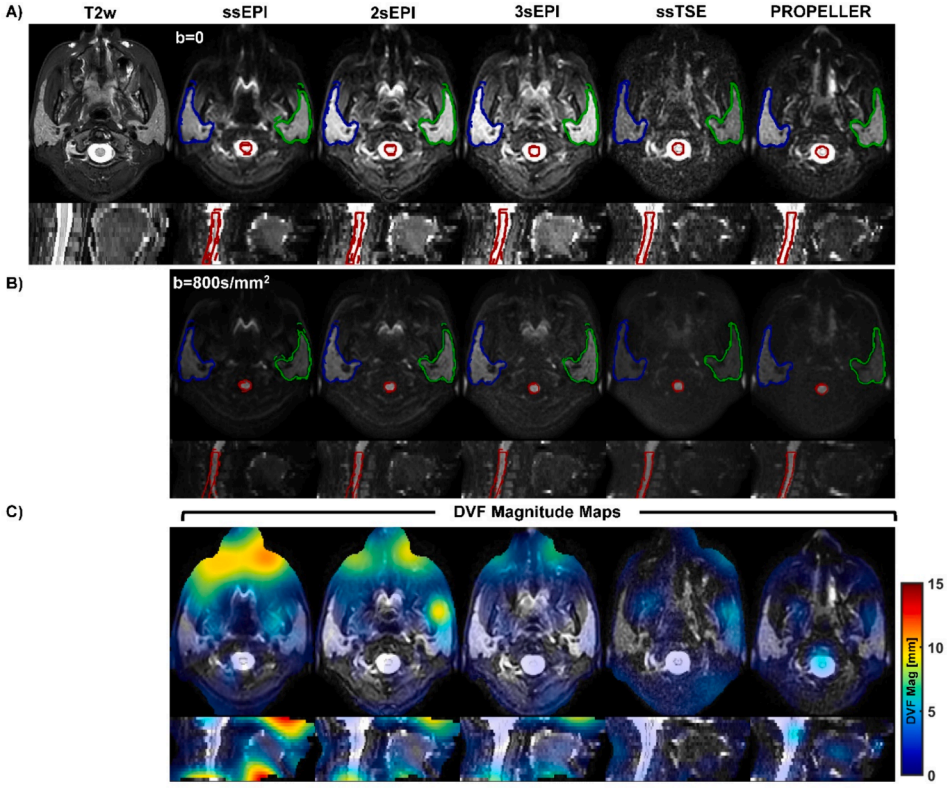

Fig. 2. Images acquired with each DWI protocol are shown in comparison with a non-DWI T2-weighted (T2w) sequence for b = 0 (A) and b = 800 s/mm^2 (B). Displacement vector field (DVF) maps computed from a deformable registration between each DWI scan and the T2w reference are also overlaid (C). All DWI are displayed with all averages included (number of signal averages = 3 for PROPELLER, 5 for all others). Distortions were clearly visible in the nasal cavity and inferior spinal cord for ssEPI which were reduced in 2sEPI, further reduced in 3sEPI, and largely eliminated with ssTSE and PROPELLER.

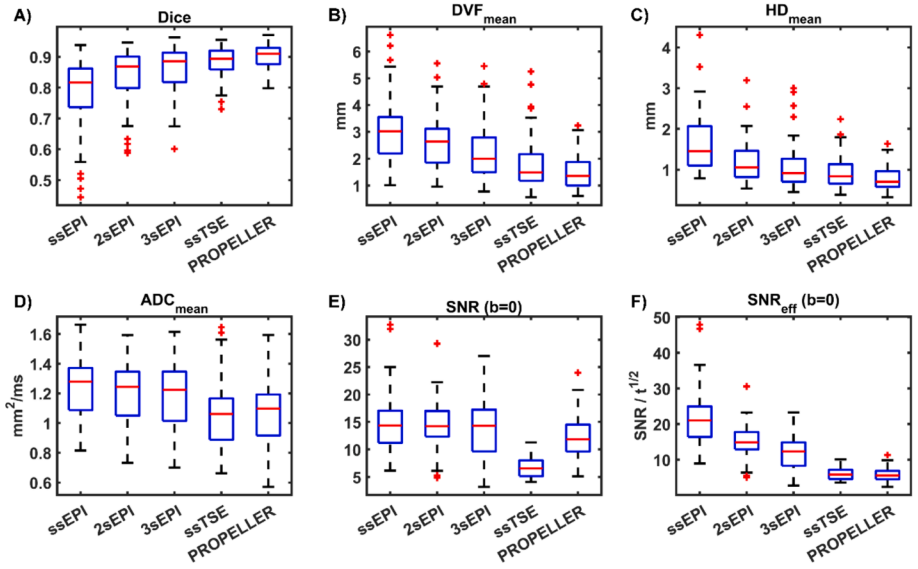

Fig. 3. Summary of results from volunteer image distortion (A, B, C), ADC mapping (D), and SNR / SNR efficiency (SNR_{eff} = SNR divided by the square root of scan time) analysis based on b = 0 images (E, F). Boxplots indicate the median (red center line), lower and upper quartiles (blue box) and range (black whiskers and/or red plus signs where outliers were present).

(2sEPI showed significantly less distortion than ssEPI in all metrics except for DVF_{mean}). DVF_{mean} and HD_{mean} were < 1 mm for all methods besides ssEPI and 2sEPI and both DVF_{95} and HD_{95} (indicators of "worst-case" distortions) were < 2 mm for all methods besides ssEPI.

All methods quantified phantom ADC accurately with biases ≤ 0.03x10^{-3}mm^2/s. Slightly (but statistically significant) lower biases were observed for 2sEPI and 3sEPI vs. ssEPI (bias = -0.01 ± 0.06 and −0.02 ± 0.07x10^{-3}mm^2/s, respectively). ADC repeatability was < 3 % for all methods, and interscan correlation coefficients were all > 0.99, but the best repeatability was observed for ssTSE and PROPELLER (wCV=0.5 % and 0.8 %, respectively vs. 2.6 %, 1.4 %, 2.7 % for ssEPI, 2sEPI, 3sEPI, respectively).

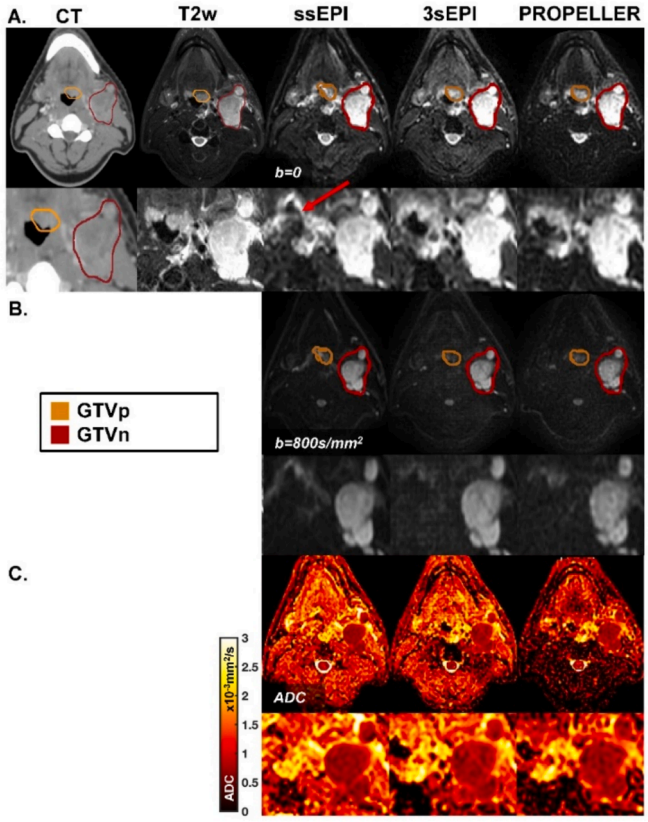

Fig. 4. Example images acquired in a patient with human papilloma virus associated (HPV+) oropharyngeal cancer with (A) CT, T2-weighted (T2w) MRI, and DWI b = 0 images with single-shot EPI (ssEPI), multi-shot EPI with 3 shots (3sEPI), and Periodically Rotated Overlapping ParallEL Lines with Enhanced Reconstruction (PROPELLER), (B) corresponding b = 800 s/mm^2 DWI, and (C) apparent diffusion coefficient (ADC) maps reconstructed from each DWI technique. All DWI are displayed with all averages included (number of signal averages = 3 for PROPELLER, 5 for all others). Radiotherapy treatment planning is based primarily on CT imaging, but the soft-tissue contrast of MRI improves anatomic visualization including gross tumor (e.g., primary tumor – orange outline, nodal disease – red outline). ADC mapping with DWI can depict further tumor detail due to reduced diffusivity in high cell-density areas, but with conventional ssEPI substantial distortions (red arrow) make it unsuitable for direct use in planning. Distortions were largely eliminated with 3sEPI and PROPELLER. 3sEPI also maintained similar ADC mapping to 3sEPI, but PROPELLER showed significantly lower ADC values, particularly outside the tumor in regions of muscle.

3.2. Volunteer imaging

Images and DVF maps from a healthy volunteer are shown in Fig. 2. For ssEPI, distortions and elevated DVF magnitudes were visible in the nasal cavity and inferior spinal cord. Distortions were reduced with 2sEPI, and further removed with 3sEPI, ssTSE, and PROPELLER.

When computed across all volunteers, significant differences in Dice coefficient and DVF magnitude were observed between sequences (Fig. 3, Supplementary Table S2). Across all structures, average Dice coefficients were: ssEPI=0.79 ± 0.11, 2sEPI=0.85 ± 0.08, 3sEPI=0.86 ± 0.07, ssTSE=0.88 ± 0.05, PROPELLER=0.90 ± 0.04, and mean displacements were: ssEPI=3.06 ± 1.25 mm, 2sEPI=2.62 ± 0.99 mm, 3sEPI=2.21 ± 0.98 mm, ssTSE=1.78 ± 0.94 mm, PROPELLER=1.49 ± 0.63 mm. Compared with ssEPI, all methods showed significantly higher Dice coefficients ($P<1x10^{-3}$) and significantly lower DVF_{mean} ($P<1x10^{-3}$). PROPELLER exhibited the lowest distortions of all methods in terms of both structure agreement and DVF magnitude. Results for individual structures are reported in Supplementary Fig. S1.

ADC and SNR measurements from all volunteers and structures are shown in Fig. 3D-F. Small (but significant, $P<1x10^{-3}$) decreases in ADC were observed for 2sEPI (ADC_{mean} = 1.20 ± 0.19x10^{-3} mm^2/s) and 3sEPI (ADC_{mean} = 1.20 ± 0.21x10^{-3} mm^2/s) compared with ssEPI (ADC_{mean} = 1.25 ± 0.19x10^{-3} mm^2/s). Larger ADC decreases were observed for ssTSE (ADC_{mean} = 1.06 ± 0.23x10^{-3} mm^2/s) and PROPELLER (ADC_{mean} = 1.07 ± 0.24x10^{-3} mm^2/s). SNR_{eff} for b = 0 was highest for ssEPI (21.9 ± 7.9), decreased significantly ($P<1x10^{-3}$) with 2sEPI (15.1 ± 5.0) and 3sEPI (12.1 ± 4.5), and was lowest with ssTSE (6.0 ± 1.6), and PROPELLER (5.7 ± 1.91). SNR_{eff} values from b = 200 and 800 s/mm^2 images are plotted in Supplementary Fig. S2.

3.3. Patient imaging

Fig. 4 shows images and ADC maps from a patient with HPV+OPC. Distortions near the primary tumor (near the airway) were apparent with ssEPI but were not seen for 3sEPI or PROPELLER. ADC maps appeared similar between ssEPI and 3sEPI, but lower ADC values were observed for PROPELLER, particularly in posterior neck muscle.

Summary statistics for patient GTV are shown in Fig. 5 and Supplementary Table S3. As in volunteer studies, 3sEPI and PROPELLER demonstrated lower distortions than ssEPI in Dice and DVF analyses. While many of the differences were not statistically significant, the trends were consistent with volunteer data, and the lack of statistical significance likely stems from the small sample size of the patient study (N=5). ADC values did not differ significantly in GTVp or GTVn between ssEPI and 3sEPI but were significantly lower in GTVp with PROPELLER (P=0.02).

In one patient, 3sEPI scans with b > 0 exhibited visible ghosting that was not present in ssEPI or PROPELLER scans (Supplementary Fig. S3). Because this artifact was also not visible in the 3sEPI b = 0 scan, this was

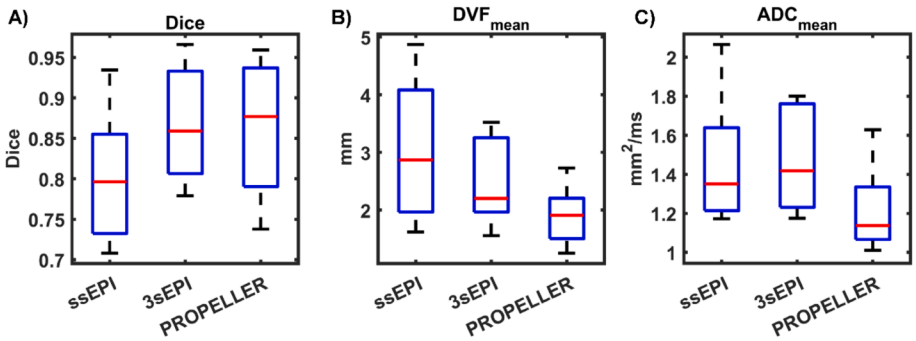

Fig. 5. Summary of results from patient gross tumor volumes (GTV) including image distortion (A, B) and ADC mapping (C) analysis based on b = 0 images. Boxplots indicate the median (red center line), lower and upper quartiles (blue box) and range (black whiskers and/or red plus signs where outliers were present). Data from both nodal and primary GTV are included in all plots.

likely caused by motion during diffusion encoding that was not fully corrected by the phase-navigator during multi-shot reconstruction.

4. Discussion

Applications of MRI in radiotherapy treatment planning require stricter geometric accuracy than diagnostic applcations. Treatment planning images guide the delineation of tumors and normal tissues which determine the spatial dose distribution delivered to patients. As a result, distorted planning images can lead to geographic target misses, which may compromise tumor control and increase doses to normal tissues. With these factors in mind, AAPM Task Group 284, which addressed the use of MRI in radiotherapy simulation, noted that geometric distortions should be minimized with a recommended tolerance of $\leq$ 2 mm[14]. Our results (and findings of others[13]) indicate that ssEPI DWI distortions can exceed this tolerance in HN and is therefore not suitable for direct use in treatment planning. In agreement with prior studies[17], we found that ssTSE dramatically reduced distortion compared with ssEPI. However, compared with EPI sequences, substantial SNR reduction were observed with ssTSE despite 3-fold scan time increases, leading to biased ADC values *in vivo*.

3sEPI strikes a good balance for radiotherapy applications by alleviating distortions while maintaining similar SNR and *in vivo* ADC values to ssEPI. 3sEPI yielded average distortions $\sim$ 2 mm *in-vivo* and $<$ 2 mm in phantom while maintaining substantially higher SNR efficiency than ssTSE or PROPELLER. This indicates that higher spatial resolutions and/or higher b-values may be feasible. With msEPI, the number of shots is directly proportional to scan time and inversely correlated with distortions due to higher bandwidths enabled by shortened readouts (Table 1). Further bandwidth increases and distortion reductions are likely feasible with $>$ 3 shots, but this must be balanced against clinically acceptable scan times. When moving to very high spatial resolutions and/or numbers of shots, msEPI may permit significantly shorter TEs than ssEPI, which could offset the scan time increases by allowing reductions in signal averages.

One key limitation of msEPI is the potential for increased motion sensivitiy due to inter-shot phase inconsistencies from motion. Our acquisitions used phase-navigators[20,24] to correct for this, but these may not be fully effective for complex motion[28]. This may explain the ghosting artifacts observed in one patient for 3sEPI near swallowing structures with b = 200 and 800 s/mm^2 (Supplementary Fig. S2), though similar artifacts were not observed elsewhere in this study. Improved motion robustness in msEPI may also be achieved using motion compensated diffusion encoding[28,29] or careful rejection of corrupted data[20,30].

PROPELLER DWI demonstrated very low levels of distortion, comparable to ssTSE, while improving absolute SNR, with unchanged SNR_{eff} (Fig. 3). PROPELLER has several advantages compared with ssTSE that are beneficial for radiotherapy. First, PROPELLER has inherent motion robustness due to non-Cartesian oversampling of central k-space which may be important for the longer scan times required with any TSE-based acquisition. Second, PROPELLER acquisitions permit higher spatial resolutions than ssTSE without excessively long individual readouts (less blurring). However, the negative *in vivo* ADC bias observed for both ssTSE and PROPELLER indicate that noise-floor effects may be affecting high b-value images [31] and suggests that higher spatial resolutions and/or b-values may be difficult to achieve with either technique. While future innovations in hardware and/or reconstruction could improve SNR_{eff} and make PROPELLER/ssTSE more practical, msEPI appears to be a well-balanced solution given current technology.

Other studies demonstrated reduced distortion in HN DWI with msEPI[32–36], ssTSE[17,32,37–42], and PROPELLER[32,34] acquisitions. A few studies also performed similar intercomparisons between msEPI, ssTSE, and/or PROPELLER scans[32,34,43,44], which agreed with our finding that TSE-based acquisitions result in comparatively less distortion than msEPI. However, these studies relied on qualitative distortion comparisons[33,38,39,42,43], inter-image correlations[36], 2-dimensional distortion measurements[34,35,40,41,44], or phantom-based distortion measurements[32,37]. While these methods are sufficient for comparing techniques, validating these techniques for radiotherapy requires knowledge of local and 3-dimensional distortions *in vivo*. To our knowledge, only Schakel et al. reported on 3-dimensional *in-vivo* distortions for ssEPI and ssTSE[13,17] by computing expected voxel shifts based on B_0 maps. For ssEPI, the reported median displacements (3.2 mm in GTVs) were in agreement with our findings (3.0/3.1 mm in GTVn/GTVp, respectively). We believe that our image-based distortion quantification improved upon this analysis by incorporating additional complexities that manifest in real images but are not captured in B_0 field analysis such as eddy currents and gradient nonlinearities.

There are some limitations in our study. First, ADC repeatability analysis was only assessed in phantom. Future studies will focus on quantifying repeatability for these alternative techniques, as has been done previously for similar sequences[32,45]. Second, much of our distortion analysis was based on deformable image registration between DWI and T2-weighted MRI scans. Deformable registration carries uncertainties and it is possible that our results would have varied with a different algorithm. However, we found very similar distortion trends using contour analysis which were entirely independent from deformable registrations. Furthermore, it is possible that the T2-weighted reference scan had some distortions, although no visible evidence of distortions was observed in comparison with CT in patient scans (Supplementary Fig. S4). Lastly, this analysis focused on 3.0 T imaging and the tradeoffs are likely different for lower field strengths, where distortions are less severe and SNR is lower. Both factors may improve the viability of ssEPI and make TSE-based acquisitions more challenging at 1.5 T.

In conclusion, DWI acquisitions with 3-shot EPI appear promising for HN radiotherapy planning. Significant distortion reductions were observed compared with ssEPI, but with superior SNR efficiency and *in vivo* ADC quantification to ssTSE and PROPELLER.

Funding Statement

This research was funded in part through the NIH/NCI Cancer Center Support Grant P30 CA008748.

Declaration of competing interest

The authors declare the following financial interests/personal relationships which may be considered as potential competing interests: Nancy Lee receives consulting fees from Shanghai Joanne Medical Ltd, Yingming Consulting, and Varian, has support from a Varian travel grant, and is on the advisory board for Merck, Merck Serono, Merck EMD, Nanobiotix, and Regeneron. Alex Dresner is a Philips Healthcare employee. This study was conducted under a research agreement with Philips.

Appendix A. Supplementary data

Supplementary data to this article can be found online at https://doi.org/10.1016/j.phro.2024.100653.

References

[1] White NS, McDonald C, Farid N, Kuperman J, Karow D, Schenker-Ahmed NM, et al. Diffusion-weighted imaging in cancer: physical foundations and applications of restriction spectrum imaging. Cancer Res 2014;74:4638–52. https://doi.org/10.1158/0008-5472.CAN-13-3534.

[2] Surov A, Meyer HJ, Wienke A. Correlation between apparent diffusion coefficient (ADC) and cellularity is different in several tumors: a meta-analysis. Oncotarget 2017;8:59492. https://doi.org/10.18632/ONCOTARGET.17752.

[3] Hatakenaka M, Nakamura K, Yabuuchi H, Shioyama Y, Matsuo Y, Ohnishi K, et al. Pretreatment apparent diffusion coefficient of the primary lesion correlates with local failure in head-and-neck cancer treated with chemoradiotherapy or

radiotherapy. International Journal of Radiation Oncology*Biology*Physics 2011; 81:339–45. https://doi.org/10.1016/J.IJROBP.2010.05.051.
[4] Martens RM, Noij DP, Koopman T, Zwezerijnen B, Heymans M, de Jong MC, et al. Predictive value of quantitative diffusion-weighted imaging and 18-F-FDG-PET in head and neck squamous cell carcinoma treated by (chemo)radiotherapy. Eur J Radiol 2019;113:39–50. https://doi.org/10.1016/J.EJRAD.2019.01.031.
[5] Martens RM, Koopman T, Lavini C, Ali M, Peeters CFW, Noij DP, et al. Multiparametric functional MRI and 18F-FDG-PET for survival prediction in patients with head and neck squamous cell carcinoma treated with (chemo) radiation. Eur Radiol 2021;31:616–28. https://doi.org/10.1007/S00330-020-07163-3.
[6] Matoba M, Tuji H, Shimode Y, Toyoda I, Kuginuki Y, Miwa K, et al. Fractional change in apparent diffusion coefficient as an imaging biomarker for predicting treatment response in head and neck cancer treated with chemoradiotherapy. AJNR Am J Neuroradiol 2014;35:379–85. https://doi.org/10.3174/AJNR.A3706.
[7] Wong KH, Panek R, Dunlop A, Mcquaid D, Riddell A, Welsh LC, et al. Changes in multimodality functional imaging parameters early during chemoradiation predict treatment response in patients with locally advanced head and neck cancer. Eur J Nucl Med Mol Imaging 2018;45:759–67. https://doi.org/10.1007/S00259-017-3890-2/FIGURES/3.
[8] Paudyal R, Oh JH, Riaz N, Venigalla P, Li J, Hatzoglou V, et al. Intravoxel incoherent motion diffusion-weighted MRI during chemoradiation therapy to characterize and monitor treatment response in human papillomavirus head and neck squamous cell carcinoma. J Magn Reson Imaging 2017;45:1013–23. https://doi.org/10.1002/JMRI.25523.
[9] Vandecaveye V, Dirix P, De Keyzer F, Op De Beeck K, Vander Poorten V, Roebben I, et al. Predictive value of diffusion-weighted magnetic resonance imaging during chemoradiotherapy for head and neck squamous cell carcinoma. Eur Radiol 2010; 20:1703–14. https://doi.org/10.1007/S00330-010-1734-6/FIGURES/6.
[10] Freihat O, Pinter T, Kedves A, Sipos D, Cselik Z, Repa I, et al. Diffusion-Weighted Imaging (DWI) derived from PET/MRI for lymph node assessment in patients with Head and Neck Squamous Cell Carcinoma (HNSCC). Cancer Imaging 2020;20: 1–12. https://doi.org/10.1186/S40644-020-00334-X/FIGURES/8.
[11] Dirix P, Haustermans K, Vandecaveye V. The value of magnetic resonance imaging for radiotherapy planning. Semin Radiat Oncol 2014;24:151–9. https://doi.org/10.1016/j.semradonc.2014.02.003.
[12] Houweling AC, Wolf AL, Vogel WV, Hamming-Vrieze O, Van Vliet-Vroegindeweij C, Van De Kamer JB, et al. FDG-PET and diffusion-weighted MRI in head-and-neck cancer patients: implications for dose painting. Radiother Oncol 2013;106:250–4. https://doi.org/10.1016/J.RADONC.2013.01.003.
[13] Schakel T, Hoogduin JM, Terhaard CHJ, Philippens MEP. Diffusion weighted MRI in head-and-neck cancer: geometrical accuracy. Radiother Oncol 2013;109:394–7. https://doi.org/10.1016/J.RADONC.2013.10.004.
[14] Glide-Hurst CK, Paulson ES, McGee K, Tyagi N, Hu Y, Balter J, et al. Task group 284 report: magnetic resonance imaging simulation in radiotherapy: considerations for clinical implementation, optimization, and quality assurance. Med Phys 2021;48:e636–70. https://doi.org/10.1002/MP.14695.
[15] Alsop DC. Phase insensitive preparation of single-shot RARE: application to diffusion imaging in humans. Magn Reson Med 1997;38:527–33. https://doi.org/10.1002/MRM.1910380404.
[16] Schick F. SPLICE: Sub-second diffusion-sensitive MR imaging using a modified fast spin-echo acquisition mode. Magn Reson Med 1997;38:638–44. https://doi.org/10.1002/MRM.1910380418.
[17] Schakel T, Hoogduin JM, Terhaard CHJ, Philippens MEP. Technical Note: Diffusion-weighted MRI with minimal distortion in head-and-neck radiotherapy using a turbo spin echo acquisition method. Med Phys 2017;44:4188–93. https://doi.org/10.1002/MP.12363.
[18] Kooreman ES, van Houdt PJ, Keesman R, Pos FJ, van Pelt VWJ, Nowee ME, et al. ADC measurements on the Unity MR-linac - A recommendation on behalf of the Elekta Unity MR-linac consortium. Radiother Oncol 2020;153:106–13. https://doi.org/10.1016/j.radonc.2020.09.046.
[19] Klüter S. Technical design and concept of a 0.35 T MR-Linac. Clin Transl. Radiat Oncol 2019;18:98–101. https://doi.org/10.1016/j.ctro.2019.04.007.
[20] Porter DA, Heidemann RM. High resolution diffusion-weighted imaging using readout-segmented echo-planar imaging, parallel imaging and a two-dimensional navigator-based reacquisition. Magn Reson Med 2009;62:468–75. https://doi.org/10.1002/mrm.22024.
[21] Chen NK, Guidon A, Chang HC, Song AW. A robust multi-shot scan strategy for high-resolution diffusion weighted MRI enabled by multiplexed sensitivity-encoding (MUSE). Neuroimage 2013;72:41. https://doi.org/10.1016/J.NEUROIMAGE.2013.01.038.
[22] Pipe JG, Farthing VG, Forbes KP. Multishot diffusion-weighted FSE using PROPELLER MRI. Magn Reson Med 2002;47:42–52.
[23] Deng J, Virmani S, Young J, Harris K, Yang GY, Rademaker A, et al. Diffusion-weighted PROPELLER MRI for quantitative assessment of liver tumor necrotic fraction and viable tumor volume in VX2 rabbits. J Magn Reson Imaging 2008;27: 1069–76. https://doi.org/10.1002/jmri.21327.
[24] Jeong H-K, Gore JC, Anderson AW. High-resolution human diffusion tensor imaging using 2-D navigated multishot SENSE EPI at 7 T. Magn Reson Med 2013; 69:793–802. https://doi.org/10.1002/mrm.24320.
[25] Alliance QIB. QIBA profile: Diffusion-weighted magnetic resonance imaging (DWI). Profile Consensus (QIBA) 2019.
[26] Klein S, Staring M, Murphy K, Viergever MA, Pluim JP. elastix: a toolbox for intensity-based medical image registration. IEEE Trans Med Imaging 2010;29: 196–205. https://doi.org/10.1109/TMI.2009.2035616.
[27] Shukla-Dave A, Obuchowski NA, Chenevert TL, Jambawalikar S, Schwartz LH, Malyarenko D, et al. Quantitative imaging biomarkers alliance (QIBA) recommendations for improved precision of DWI and DCE-MRI derived biomarkers in multicenter oncology trials. J Magn Reson Imaging 2019;49:e101–21. https://doi.org/10.1002/jmri.26518.
[28] Geng R, Zhang Y, Rice J, Muehler MR, Starekova J, Rutkowski DR, et al. Motion-robust, blood-suppressed, reduced-distortion diffusion MRI of the liver. Magn Reson Med 2022. https://doi.org/10.1002/mrm.29531.
[29] Hannum AJ, Cork TE, Setsompop K, Ennis DB. Phase stabilization with motion compensated diffusion weighted imaging. Magn Reson Med 2024. https://doi.org/10.1002/mrm.30218.
[30] Lee PK, Zhou X, Hargreaves BA. Robust multishot diffusion-weighted imaging of the abdomen with region-based shot rejection. Magn Reson Med 2024. https://doi.org/10.1002/mrm.30102.
[31] Gudbjartsson H, Patz S. The Rician distribution of noisy MRI data. Magn Reson Med 1995;34:910–4. https://doi.org/10.1002/mrm.1910340618.
[32] McDonald BA, Salzillo T, Mulder S, Ahmed S, Dresner A, Preston K, et al. Prospective evaluation of in vivo and phantom repeatability and reproducibility of diffusion-weighted MRI sequences on 1.5 T MRI-linear accelerator (MR-Linac) and MR simulator devices for head and neck cancers. Radiother Oncol 2023;185: 109717. Doi: 10.1016/j.radonc.2023.109717.
[33] Bae YJ, Choi BS, Jeong H-K, Sunwoo L, Jung C, Kim JH. Diffusion-Weighted Imaging of the Head and Neck: Influence of Fat-Suppression Technique and Multishot 2D Navigated Interleaved Acquisitions. AJNR Am J Neuroradiol 2018; 39:145–50. https://doi.org/10.3174/ajnr.A5426.
[34] Kida I, Ueguchi T, Matsuoka Y, Zhou K, Stemmer A, Porter D. Comparison of Diffusion-Weighted Imaging in the Human Brain Using Readout-Segmented EPI and PROPELLER Turbo Spin Echo With Single-Shot EPI at 7 T MRI. Invest Radiol 2016;51:435–9. https://doi.org/10.1097/RLI.0000000000000248.
[35] Koyasu S, Iima M, Umeoka S, Morisawa N, Porter DA, Ito J, et al. The clinical utility of reduced-distortion readout-segmented echo-planar imaging in the head and neck region: initial experience. Eur Radiol 2014;24:3088–96. https://doi.org/10.1007/s00330-014-3369-5.
[36] Konar AS, Fung M, Paudyal R, Oh JH, Mazaheri Y, Hatzoglou V, et al. Diffusion-weighted echo planar imaging using multiplexed sensitivity encoding and reverse polarity gradient in head and neck cancer: an initial study. Tomography 2020;6: 231–40. https://doi.org/10.18383/j.tom.2020.00014.
[37] Gao Y, Han F, Zhou Z, Cao M, Kaprealian T, Kamrava M, et al. Distortion-free diffusion MRI using an MRI-guided Tri-Cobalt 60 radiotherapy system: sequence verification and preliminary clinical experience. Med Phys 2017;44:5357–66. https://doi.org/10.1002/mp.12465.
[38] Verhappen MH, Pouwels PJW, Ljumanovic R, Van Der Putten L, Knol DL, De Bree R, et al. Diffusion-weighted MR imaging in head and neck cancer: comparison between half-fourier acquired single-shot Turbo Spin-Echo and EPI techniques. AJNR Am J Neuroradiol 2012;33:1239–46. https://doi.org/10.3174/AJNR.A2949.
[39] Gumeler E, Parlak S, Yazici G, Karabulut E, Kiratli H, Oguz KK. Single shot echo planar imaging (ssEPI) vs single shot turbo spin echo (ssTSE) DWI of the orbit in patients with ocular melanoma. Br J Radiol 2021;94:20200825. https://doi.org/10.1259/bjr.20200825.
[40] Hirata K, Nakaura T, Okuaki T, Kidoh M, Oda S, Utsunomiya D, et al. Comparison of the image quality of turbo spin echo- and echo-planar diffusion-weighted images of the oral cavity. Medicine 2018;97:e0447.
[41] Mikayama R, Yabuuchi H, Sonoda S, Kobayashi K, Nagatomo K, Kimura M, et al. Comparison of intravoxel incoherent motion diffusion-weighted imaging between turbo spin-echo and echo-planar imaging of the head and neck. Eur Radiol 2018; 28:316–24. https://doi.org/10.1007/s00330-017-4990-x.
[42] Pokorney AL, Miller JH, Hu HH. Comparison of 2D single-shot turbo-spin-echo and spin-echo echo-planar diffusion weighted brain MRI at 3.0 Tesla: preliminary experience in children. Clin Imaging 2017;42:152–7. Doi: 10.1016/j.clinimag.2016.12.005.
[43] Sheng Y, Hong R, Sha Y, Zhang Z, Zhou K, Fu C. Performance of TGSE BLADE DWI compared with RESOLVE DWI in the diagnosis of cholesteatoma. BMC Med Imaging 2020;20:40. https://doi.org/10.1186/s12880-020-00438-7.
[44] Fu Q, Kong X-C, Liu D-X, Zhou K, Guo Y-H, Lei Z-Q, et al. Turbo gradient and spin echo PROPELLER-diffusion weighted imaging for orbital tumors: a comparative study with readout-segmented echo-planar imaging. Front Neurosci 2021;15: 755327. https://doi.org/10.3389/fnins.2021.755327.
[45] Paudyal R, Konar AS, Obuchowski NA, Hatzoglou V, Chenevert TL, Malyarenko DI, et al. Repeatability of quantitative diffusion-weighted imaging metrics in phantoms, head-and-neck and thyroid cancers: preliminary findings. Tomography 2019;5:15–25. https://doi.org/10.18383/j.tom.2018.00044.